8B.4 Mesoscale Ensemble Sensitivity of Dryline Convection Initiation

Aaron J. Hill*
Texas Tech University, Lubbock, Texas

Christopher C. Weiss, Brian C. Ancell
Texas Tech University, Lubbock, Texas

1. INTRODUCTION

Recent advancements in numerical weather prediction (NWP), including improved data assimilation procedures and increased computing power for higher resolution simulations, have improved the timing and location forecasts of dryline convection initiation (CI). Limitations still exist, however, due to the complexity of convection; small scale kinematic processes that are not well-resolved and microphysical interactions. Furthermore, the trend in NWP has been to translate the improvements in deterministic forecasting to ensemble prediction. The use of ensembles for dryline CI forecasts provides an estimate of uncertainty for the intensity, location, timing, and duration of severe storms.

Further improvements can be made to forecasts through the understanding of initial condition errors and their growth during model integration, typically achieved through sensitivity analysis. Adjoint sensitivity has been utilized (Rabier et al. 1996; Zou et al. 1998) to gain understanding of where perturbations in initial conditions have the potential to grow rapidly to impact a chosen forecast metric (R), or response function. Limitations with this method exist, however, including the need for the model and parameterizations to be differentiable, less accuracy for longer lead times and larger perturbations, and it only provides information on dynamic error growth; there is no information used regarding the likelihood of errors in the initial state. A newer sensitivity technique, ensemble sensitivity analysis (ESA; Ancell and Hakim 2007; Hakim and Torn 2008; Torn and Hakim 2008), has been shown to reveal sensitivities to weather features rather than perturbations alone. These weather features are typically collocated with errors in the initial conditions. Thus, the ensemble-based sensitivity highlights where errors in the initial-state, tied with the evolving weather pattern, will most influence the forecast. Utilizing the output from an ensemble of deterministic forecasts, a chosen scalar forecast metric can be linearly-regressed back to the initial time, or any other forecast time, to reveal how the metric changes with perturbations in the previous states (Fig. 1). Ancell and Hakim (2007) illustrate that ensemble sensitivity is simply a result of mapping of adjoint sensitivity into the full initial time atmospheric state using ensemble covariance relationships, effectively identifying weather features that are dynamically related to the forecast metric. Sensitivity can be described as

$$\frac{\partial \boldsymbol{R}}{\partial \boldsymbol{x_i}} = \frac{\delta \boldsymbol{R} \delta x_i^T}{\delta \boldsymbol{x_i} \delta x_i^T}, \quad (1)$$

where ***R*** is the forecast metric from all ensemble members (response function), $\boldsymbol{x_i}$ is the initial state vector at a grid point, and δ represents a perturbation from the mean. Thus, the sensitivity is the slope of the linear regression between ***R*** and $\boldsymbol{x_i}$, or the quotient of the covariance between ***R*** and $\boldsymbol{x_i}$ and the variance in $\boldsymbol{x_i}$.

Primarily, ensemble sensitivity studies have been concerned with synoptic scale features: extratropical cyclones (e.g., Ancell and Hakim 2007; Torn and Hakim 2008; Garcies and Homar 2009, 2010; Chang et al. 2013; McMurdie and Ancell 2014), extratropical transition (e.g., Torn and Hakim 2009; Anwender et al. 2012), and tropical cyclones (e.g., Torn 2010; Qin and Mu 2011; Kunii et al. 2012; Ito and Wu 2013; Torn and Cook 2013; Xie et al. 2013; Torn 2014). A handful of studies have utilized ESA on mesoscale features not related to convection (Zack et al. 2010c,a,b, 2011a,b; Bednarczyk and Ancell 2014). Bednarczyk and Ancell (2014) performed ESA on a convective case from April 2012 and showed strongly sensitive features aloft related to the synoptic parent system. The primary goal of this study is to demonstrate the utility of applying ESA to dryline convection cases over North Texas to highlight dynamic, mesoscale features that have an impact on the initiating storms.

Corresponding author address: Aaron J. Hill, Texas Tech University, Atmospheric Science Group, Department of Geosciences, Lubbock, TX, 79409; e-mail: aaron.hill@ttu.edu

2. METHODOLOGY

a. Model and Assimilation Setup

An ensemble of forecasts consisting of 50 members is produced with the Weather Research and Forecasting (WRF) v3.3.1 model. The model domain consists of three one-way nested domains at 36, 12, and 4 km horizontal resolution (Fig. 2) with 38 vertical levels. The outermost domain is initialized from 0.5 degree resolution, interpolated Global Forecast System (GFS) initial conditions obtained from the National Centers for Environmental Prediction (NCEP). Boundary conditions are initially generated from perturbed GFS initial conditions to generate the ensemble (Torn et al. 2006), where each member maintains an independent boundary condition. Later BCs are taken from GFS forecasts. Various parameterizations are employed to model small-scale, unresolved processes (Table 1). However, due to fine resolution (4 km), convection is explicitly resolved without a parameterization on the third domain (Bryan et al. 2003).

The ensemble adjustment Kalman filter (EAKF; Anderson 2001) is employed for filtering with the Data Assimilation Research Testbed (DART; Anderson et al. 2009). To properly develop flow-dependent covariances a 6-hourly assimilation cycle is completed on all domains for a 48-hour period prior for forecast initialization. The coarsest domain is initially cycled for 24 hours before the 12 and 4 km domains are initialized using the WRF model nestdown capability and cycled for the remaining 24 hours. Conventional observations are assimilated (e.g. land-surface stations, METAR, satellite winds, radiosondes, marine, and mesonet) at all cycle times. Spatially and temporally adapting covariance inflation (Anderson 2007, 2009) is employed to account for under-dispersion of the ensemble. Furthermore, observation influences are restricted to a finite distance from the observation location using covariance localization (Anderson 2001) with the Gaspari-Cohn localization function (Gaspari and Cohn 1999).

b. Analysis Methods

The model is initialized at 0000 UTC on 15 May 2013 and a 24-hour forecast is generated, valid through 0000 UTC on 16 May 2013. The forecast metrics chosen for analysis are maximum vertical velocity and average bulk shear from 0-6 km, both valid at forecast hour 24. Vertical velocity aims to represent convective intensity and initiation while bulk shear is a proxy for convective mode. Both metrics are defined within a region of CI in north-central Texas (response region, green rectangle in Figs. 10-15). The metrics are regressed against initial conditions at the surface (e.g. dewpoint, temperature, pressure) and aloft (e.g. temperature, geopotential height) throughout the forecast.

3. CASE STUDY

Discrete supercells developed at 2300 UTC on 15 May 2013 over north-central Texas (Fig. 3). An eastward-progressing dryline was positioned over central Texas (Fig. 4) aiding to initiate storms and was well captured by the ensemble (Fig. 5), with discrepancies in dryline placement between ensemble members. Warm advection precipitation is evident over the Arklatex border in Fig. 3, which was located in southeastern Texas earlier in the forecast. The dryline progression was driven by a developing surface low (Fig. 6) and eastward-progressing upper-level trough (not shown). The ensemble failed to develop storms along the dryline at forecast hour 23 (2300 UTC), when observations indicated supercells initiated. However, some individual members did initiate one hour later (Fig. 7), with a weak signal in the ensemble mean (Fig. 8). By forecast hour 25 (0100 UTC), the ensemble was indicating a more robust signal in simulated reflectivity (Fig. 9).

4. SENSITIVITY ANALYSIS

a. Maximum Vertical Velocity

The 24-hour forecast of vertical velocity is seen to be highly sensitive to surface features related to advective regimes, pressure troughs, and warm advection precipitation. Six hours prior to CI, a positive sensitivity to 2-meter temperature exists in central Texas, just south and southwest of the response region (Fig. 10a). This sensitive area originates from southeastern Texas near the Gulf of Mexico and advects northwestward through the forecast. The sensitivity signal would then suggest that a general increase in temperature across the area would result in an increase in the vertical velocity forecast metric, i.e. more members convecting or stronger convection. The vertical velocity forecast also appears to be highly sensitive to the developing surface pressure trough (Fig. 10b). A large swath of negative sensitivity to sea level pressure is evident in Fig. 10b along the pressure trough axis indicating that a deeper pressure field, which would increase the horizontal pressure gradient, may contribute to higher vertical velocities just six hours later at CI. One way to assess these sensitive features is by evaluating the differences between ensemble members, a technique used by Bednarczyk and Ancell (2014). Analyzing the difference in 2-meter temperature between a convecting and non-convecting ensemble member at forecast hour 18 shows a primary difference in southeastern Texas, extending northward into eastern Texas (Fig. 10c). This area was laden with warm-advection precipitation during this period and earlier in the forecast. The differences between members is highlighting the positional shifts of the precipitation and resulting cold pools. The convecting member has a southeastward shift of the precipitation, closer to the coastline, resulting in a warmer 2-meter temperature field farther into central Texas and cooler temperatures near the coast. Furthermore, using hydrostatic relationships, we see the same signal in the sea level pressure differences between the same members (Fig. 10d). A southeastward shift of precipitation in convecting members would produce a stronger cold pool towards the Texas coast resulting in higher surface pressure and vice versa inland. It is highly possible that the position of warm advection precipitation is having an impact on which members are producing convection six hours later. However, more in-depth analysis would need to be completed to sufficiently prove this interaction, which is not a primary goal of this study. Rather, the purpose of this study is to show the utility of ESA to highlight these mesoscale features.

Aloft, the vertical velocity forecast is sensitive to advective temperature regimes near the capping inversion level and upper-level trough placement and strength. At 700 mb, a negative sensitivity exists to temperature that emanates from West Texas early in the forecast towards the response region by CI (Fig. 11). The sensitive region is coherent spatially and temporally throughout the entire forecast. Just prior to CI, a capping inversion is in place over the response region at approximately 700 mb (not shown). The temperature sensitivity at hour 24 (Fig. 11f) would then suggest that a decrease in strength of the cap would promote stronger vertical velocities. Because the temperature sensitivity is traceable back to the beginning of the forecast, the ESA is highlighting an important advective feature aloft that could have a large impact on the initiation of convection. Furthermore, the vertical velocity forecast is sensitive to the position and magnitude of the upper-level low, as seen through the geopotential height fields six hours prior to CI (Fig. 12). A swath of negative sensitivity is evident in the base of the troughs at 300 and 500 mb (Fig. 12a,b), indicating that a deeper magnitude or more southward positioned trough would promote stronger vertical motion. A general area of negative (positive) sensitivity south (north) of the low center at 700 mb would indicate a positional sensitivity as well (Fig. 12c). At 850 mb the pressure trough is not well developed in the southern plains but a positional sensitivity is still apparent in the Oklahoma and Texas panhandle regions (Fig. 12d). An additional positive sensitivity south of the response region at 850 mb is a result of the previously mentioned warm advection precipitation influencing the height of the 850 mb pressure level. It is noted that a convecting member tended to displace precipitation earlier in the forecast towards the Texas coastline. The displacement resulted in higher 2-meter temperature and lower sea level pressure farther inland (Fig. 10c,d). Thus, a warmer (cooler) surface temperature in central (coastal) Texas would correspond to a higher (lower) 850 mb pressure level height, which is seen in Fig. 12d.

b. Average Bulk Shear

Sensitivity analysis is also performed on the forecast of average bulk shear in the response region at forecast hour 24. Bulk shear is chosen as a forecast metric because it can be used as a proxy for storm mode, where discrete supercells initiating along the dryline are favored in high shear environments. At the surface, the forecast is sensitive to 2-meter dewpoint six hours prior to CI (Fig. 13a) to the west and southwest of the response region. The region of sensitivity exists within the area of the developing dryline. The positive sensitivity suggests that a moistening of the atmosphere near the response region would increase the bulk shear magnitude. This can be explained because of increased confluence with a strengthening dryline near the surface. Pressure sensitivities also exist (Fig. 13b) in the domain of interest. Negative sensitivity is present near the developing surface low center while positive sensitivity covers the majority of Texas. The sensitivity signal would indicate that a strengthening surface pressure gradient would increase the shear forecast, a result of stronger return flow from the Gulf of Mexico across the domain.

Sensitivities also exist aloft, similarly to the forecast of maximum vertical velocity. A strong signal of positive sensitivity to 700 mb temperature propagates from West Texas to the response region by CI (Fig. 14). The sensitivity is coherent for the entire forecast, which is indicative of a strong dynamic feature that could have an impact on the forecast. Noticeable to the west of the positive sensitivity is a region of negative sensitivity. The two are coupled and represent sensitivity to horizontal temperature gradients at 700 mb. An increase in the horizontal temperature gradient would increase the vertical wind shear through a stronger geostrophic response. Moreover, the shear forecast is strongly sensitive to the position of the upper level trough placement. A strong positional sensitivity is evident at 500 mb in Figure 15. Positive (negative) sensitivity to the east (west) illustrate that a shift westward would promote stronger shear because of a displacement of a jet maxima over the response region by forecast hour 24.

5. SUMMARY AND DISCUSSION

Ensemble sensitivity analysis has been applied on a dryline convection case from 15 May 2013. Forecasts of maximum vertical velocity and average bulk shear at convective initiation show sensitivities to features at the surface and aloft. Vertical velocities are sensitive to advective regimes of surface temperature from the Gulf of Mexico, which are coherent 0-12 hours prior to CI. A surface pressure trough is also highlighted as a sensitive feature. Moreover, the vertical velocity forecast appears highly sensitive to the placement of warm advection precipitation. Analysis of differences between convecting and non-convecting ensemble members illustrates that the precipitation and resulting cold pools may be having an impact on which members are convecting. The bulk shear forecast also was shown to be sensitive to the strength of the developing dryline and surface pressure trough. Stronger pressure gradients would result in more confluence and return flow at the surface, increasing the shear forecast to favor more discrete supercell development along the dryline. Additionally, sensitivities are evident along the dryline indicating a stronger dryline gradient, as a result of stronger surface confluence, would increase the shear magnitude. Both vertical velocity and shear showed sensitivities to upper level temperatures and troughs. A negative sensitivity to 700 mb temperature existed for vertical velocity forecasts indicating that a reduction in the capping inversion strength would favor stronger vertical velocity, i.e. more intense convection. The shear forecast was also shown to be sensitive to horizontal gradients in the 700 mb temperature field. Both magnitude and positional sensitivities were seen in the geopotential height fields, where slight differences in strength and position of the upper level troughs could impact the forecasts. Sensitivities aloft were traceable back to the beginning of the forecast, present 0-24 hours prior to CI versus the 0-12 hour sensitivity signals seen at the surface.

Linear relationships are assumed between the response functions and initial conditions. Thus, for longer forecast times, more linear forecast metrics are required. On synoptic scales where ESA has been applied more in the literature, these relationships are more valid. However, even on the mesoscale where non-linearity plays a larger role, especially with convection, this study has shown that ESA still has the ability to highlight important features that may have an impact on the forecast. ESA provides forecasters with an understanding of how initial condition errors may evolve onto the forecast. Furthermore, improvements to the forecasts can be achieved through observation targeting techniques developed from ESA theory (Ancell and Hakim 2007). The targeted observations are chosen based on their expected change to the forecast variance. However, issues still exist with observation targeting on the mesoscale due to the non-linear evolution of the atmosphere on these scales. The role of adaptive observing for convective forecasts using ESA techniques will be explored in future studies.

6. ACKNOWLEDGEMENTS

This study is funded by the NOAA CSTAR Program, grant NA11NWS4680001.

7. REFERENCES

Ancell, B. C., and G. J. Hakim, 2007: Comparing adjoint- and ensemble-sensitivity analysis with applications to observation targeting. *Mon. Wea. Rev.*, **135**, 4117–4134.

Anderson, J. L., 2001: An ensemble adjustment Kalman filter for data assimilation. *Mon. Wea. Rev.*, **129**, 2884–2903.

——, 2007: An adaptive covariance inflation error correction algorithm for ensemble filters. *Tellus A*, **59**, 210–224.

——, 2009: Spatially and temporally varying adaptive covariance inflation for ensemble filters. *Tellus A*, **61**, 72–83.

——, T. Hoar, K. Raeder, H. Liu, N. Collins, R. Torn, and A. Avellano, 2009: The data assimilation research testbed: a community facility. *Bull. Amer. Meteor. Soc.*, **90**, 1283–1296.

Anwender, D., C. Cardinali, and S. C. Jones, 2012: Data denial experiments for extratropical transition. *Tellus A*, **64**, 1–17.

Bednarczyk, C. N., and B. C. Ancell, 2014: Ensemble Sensitivity Analysis Applied to a Southern Plains Convective Event. *Mon. Wea. Rev.*, doi:10.1175/MWR-D-13-00321.1, in press.

Bryan, G. H., J. C. Wyngaard, and J. M. Fritsch, 2003: Resolution requirements for the simulation of deep moist convection. *Mon. Wea. Rev.*, **131**, 2394–2416.

Chang, E. K. M., M. Zheng, and K. Raeder, 2013: Medium-range ensemble sensitivity analysis of two extreme pacific extratropical cyclones. *Mon. Wea. Rev.*, **141**, 211–231.

Garcies, L., and V. Homar, 2009: Ensemble sensitivities of the real atmosphere: application to Mediterranean intense cyclones. *Tellus A*, **61**, 394–406.

——, and ——, 2010: An optimized ensemble sensitivity climatology of Mediterranean intense cyclones. *Nat. Hazards Earth Syst. Sci.*, **10**, 2441–2450.

Gaspari, G., and S. E. Cohn, 1999: Construction of correlation functions in two and three dimensions. *Quart J. Roy. Meteor. Soc.*, **125**, 723–757.

Hakim, G. J., and R. D. Torn, 2008: Ensemble synoptic analysis. *Synoptic—Dynamic Meteorology and Weather Analysis and Forecasting: A Tribute to Fred Sanders*, American Meteorological Society, p. 440.

Ito, K., and C.-C. Wu, 2013: Typhoon-position-oriented sensitivity analysis. Part I: Theory and verification. *J. Atmos. Sci.*, **70**, 2525–2546.

Kunii, M., T. Miyoshi, and E. Kalnay, 2012: Estimating the impact of real observations in regional numerical weather prediction using an ensemble Kalman filter. *Mon. Wea. Rev.*, **140**, 1975–1987.

McMurdie, L. A., and B. Ancell, 2014: Predictability characteristics of land-falling cyclones along the North American west coast. *Mon. Wea. Rev.*, **142**, 301–319.

Qin, X., and M. Mu, 2011: A study on the reduction of forecast error variance by three adaptive observation approaches for tropical cyclone prediction. *Mon. Wea. Rev.*, **139**, 2218–2232.

Rabier, F., E. Klinker, P. Courtier, and A. Hollingsworth, 1996: Sensitivity of forecast errors to initial conditions. *Quart J. Roy. Meteor. Soc.*, **122**, 121–150.

Torn, R. D., 2010: Ensemble-based sensitivity analysis applied to african easterly waves. *Wea. Forecasting*, **25**, 61–78.

——, 2014: The impact of targeted dropwindsonde observations on tropical cyclone intensity forecasts of four weak systems during PREDICT. *Mon. Wea. Rev.*, **142**, 2860–2878.

——, and G. J. Hakim, 2008: Ensemble-based sensitivity analysis. *Mon. Wea. Rev.*, **136**, 663–677.

——, and ——, 2009: Initial condition sensitivity of western Pacific extratropical transitions determined using ensemble-based sensitivity analysis. *Mon. Wea. Rev.*, **137**, 3388–3406.

——, and D. Cook, 2013: The role of vortex and environment errors in genesis forecasts of Hurricanes Danielle and Karl (2010). *Mon. Wea. Rev.*, **141**, 232–251.

——, G. J. Hakim, and C. Snyder, 2006: Boundary conditions for limited-area ensemble Kalman filters. *Mon. Wea. Rev.*, **134**, 2490–2502.

Xie, B., F. Zhang, Q. Zhang, J. Poterjoy, and Y. Weng, 2013: Observing strategy and observation targeting for tropical cyclones using ensemble-based sensitivity analysis and data assimilation. *Mon. Wea. Rev.*, **141**, 1437–1453.

Zack, J., E. Natenberg, S. Young, G. V Knowe, K. Waight, J. Manobianco, and C. Kamath, 2010a: *Application of ensemble sensitivity analysis to observation targeting for short-term wind speed forecasting in the Washington-Oregon region*. Tech. rep., Lawrence Livermore National Lbaratory, 65 pp., Livermore, CA.

——, ——, ——, G. Van Knowe, K. Waight, J. Manobainco, and C. Kamath, 2010b: *Application of ensemble sensitivity analysis to observation targeting for short-term wind speed forecasting in the Tehachapi region winter season*. Tech. rep., Lawrence Livermore National Laboratory, 57 pp., Livermore, CA.

——, ——, ——, J. Manobianco, and C. Kamath, 2010c: *Application of ensemble sensitivity analysis to observation targeting for short-term wind speed forecasting*. Tech. rep., Lawrence Livermore National Laboratory, 32 pp., Livermore, CA.

——, E. J. Natenberg, G. V Knowe, K. Waight, J. Manobianco, D. Hanley, and C. Kamath, 2011a: *Observing system simulation experiments (OSSEs) for the Mid-Columbia basin*. Tech. rep., Lawrence Livermore National Laboratory, 33 pp., Livermore, CA.

——, E. Natenberg, G. Knowe, J. Manobianco, K. Waight, D. Hanley, and C. Kamath, 2011b: *Use of data denial experiments to evaluate ESA forecast sensitivity patterns*. Tech. rep., Lawrence Livermore National Laboratory, 17 pp., Livermore, CA.

Zou, X., Y.-H. Kuo, and S. Low-Nam, 1998: Medium-Range Prediction of an Extratropical Oceanic Cyclone : Impact of Initial State. *Mon. Wea. Rev.*, **126**, 2737–2763.

Parameterization Type	Scheme
Boundary Layer	Yonsei University
Cumulus Convection*	Kain-Fritsch
Land Surface	Noah Land-Surface Model
Long-Wave Radiation	Rapid Radiative Transfer Model
Short-Wave Radiation	Dudhia
Microphysics	Thompson

*Convection is explicitly resolved on 4 km domain

Table 1 – Model parameterizations used to account for small-scale processes not resolved with coarser grid resolutions.

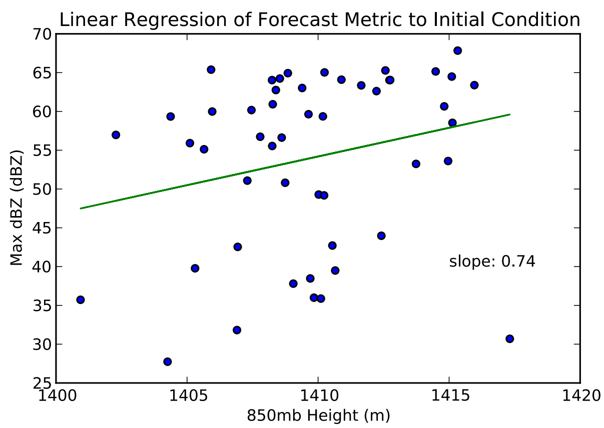

Figure 1 – Scatter (blue circles) of maximum reflectivity (dBZ) in a defined region against 850 mb geopotential height (m) at a grid point and their fitted linear regression (green line). The calculated slope represents the value of sensitivity at the grid point.

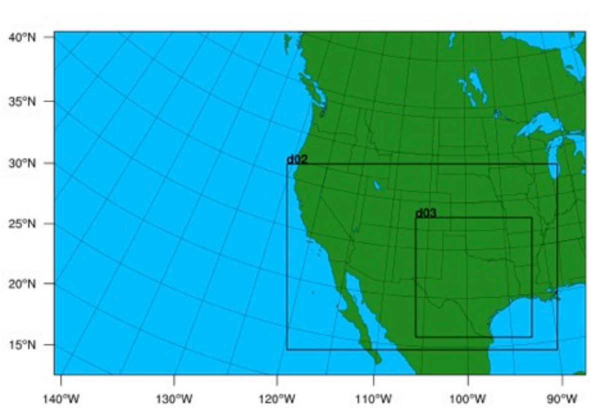

Figure 2 – WRF domain configuration with outermost domain at 36 km, d02 with 12 km, and d03 with 4 km grid resolution. Modeled after the Texas Tech University real-time ensemble system.

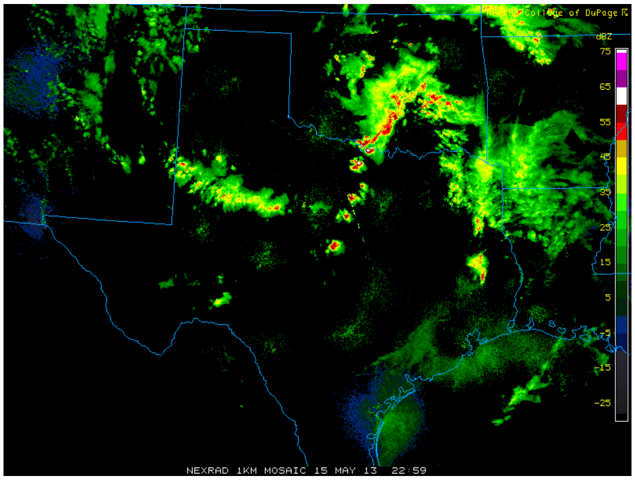

Figure 3 – Radar composite (dBZ) valid at 2300 UTC 15 May 2013 courtesy of UCAR/NCAR/MMM image archive available through http://locust.mmm.ucar.edu/

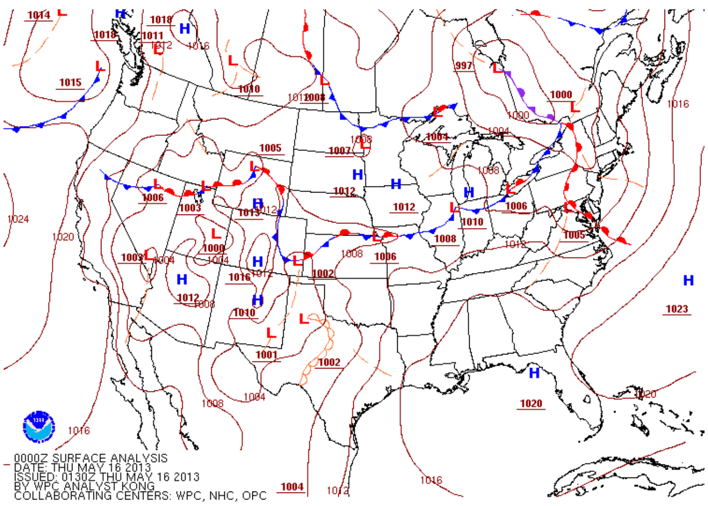

Figure 4 – Weather Prediction Center surface analysis valid at 0000 UTC 16 May 2013

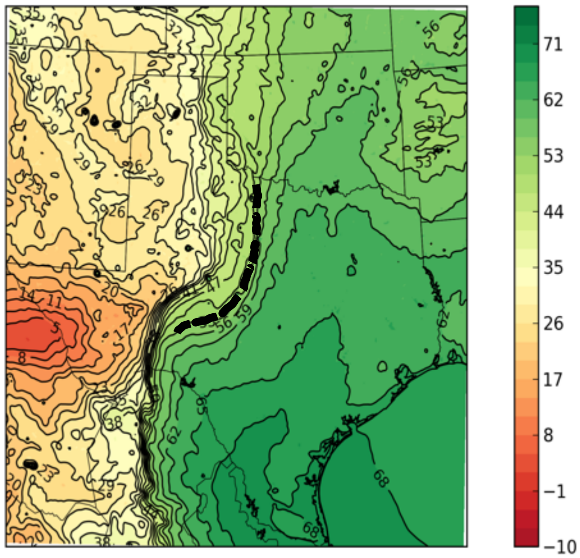

Figure 5 – Ensemble mean forecast of 2-meter dewpoint (F, shaded and contoured every 3 F) valid at 0000 UTC 16 May 2013. Black dashed line is the subjective placement of the dryline based on individual members.

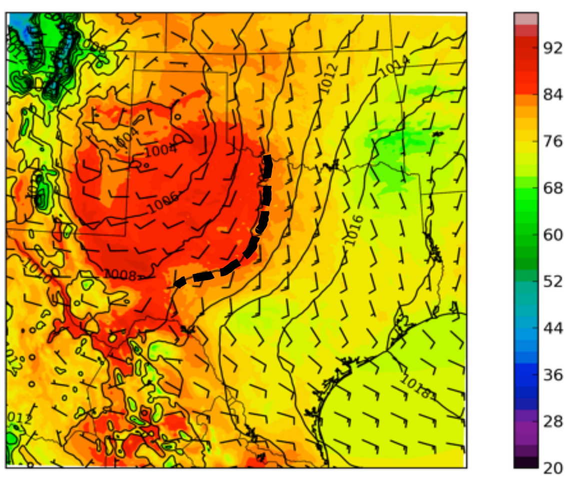

Figure 6 – Ensemble mean forecast of sea level pressure (mb, contoured every 2 mb), 2-meter temperature (F, shaded), and 10-m winds (barbs) valid at 2300 UTC 15 May 2013. Black dashed line is the same as in Fig. 5.

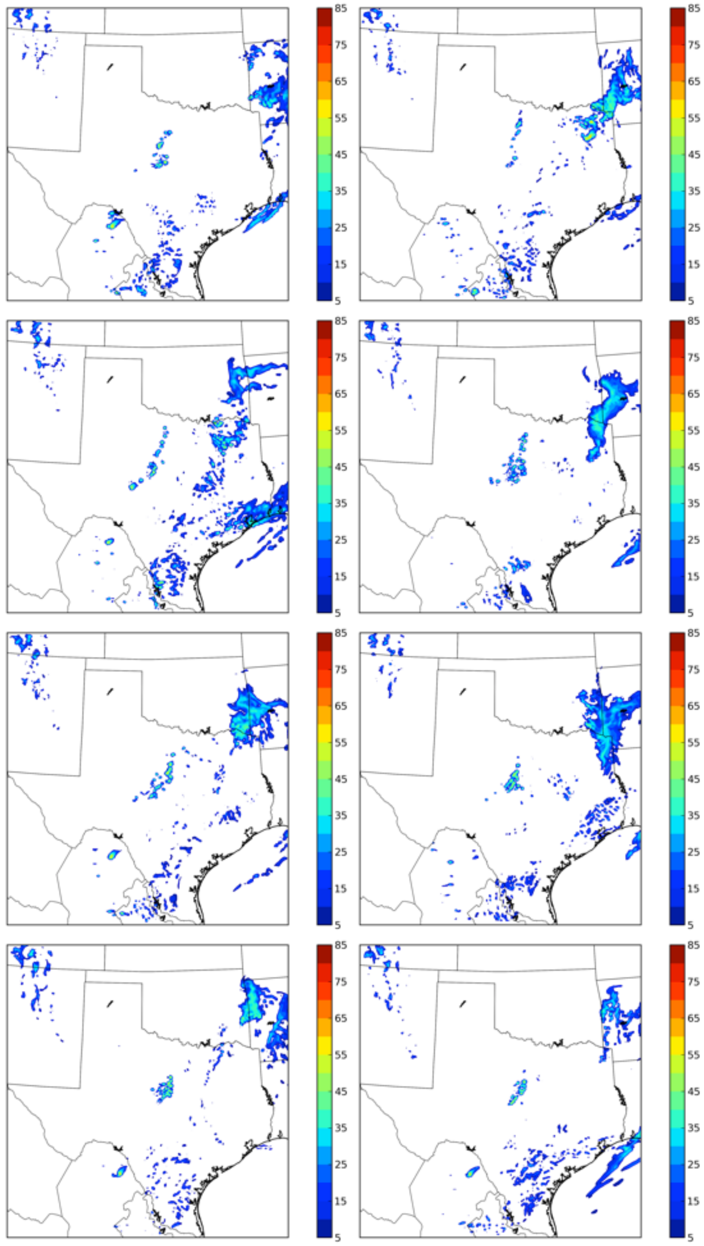

Figure 7 – Composite reflectivity (dBZ, shaded) for a selection of convecting ensemble members valid at 0000 UTC 16 May 2013.

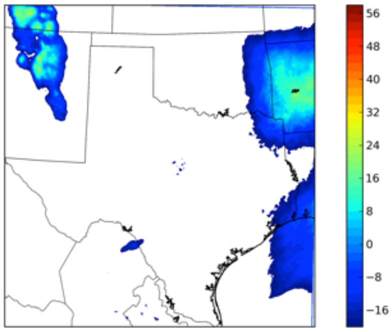

Figure 8 – Ensemble mean composite reflectivity (dBZ, shaded) valid at 0000 UTC 16 May 2013.

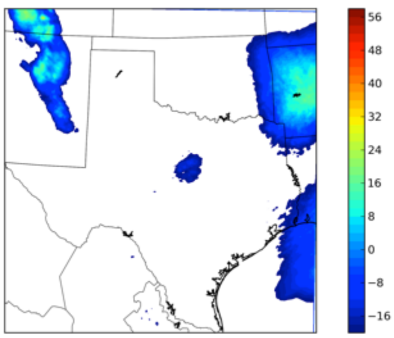

Figure 9 – Same as Fig. 8, valid at 0100 UTC 16 May 2013.

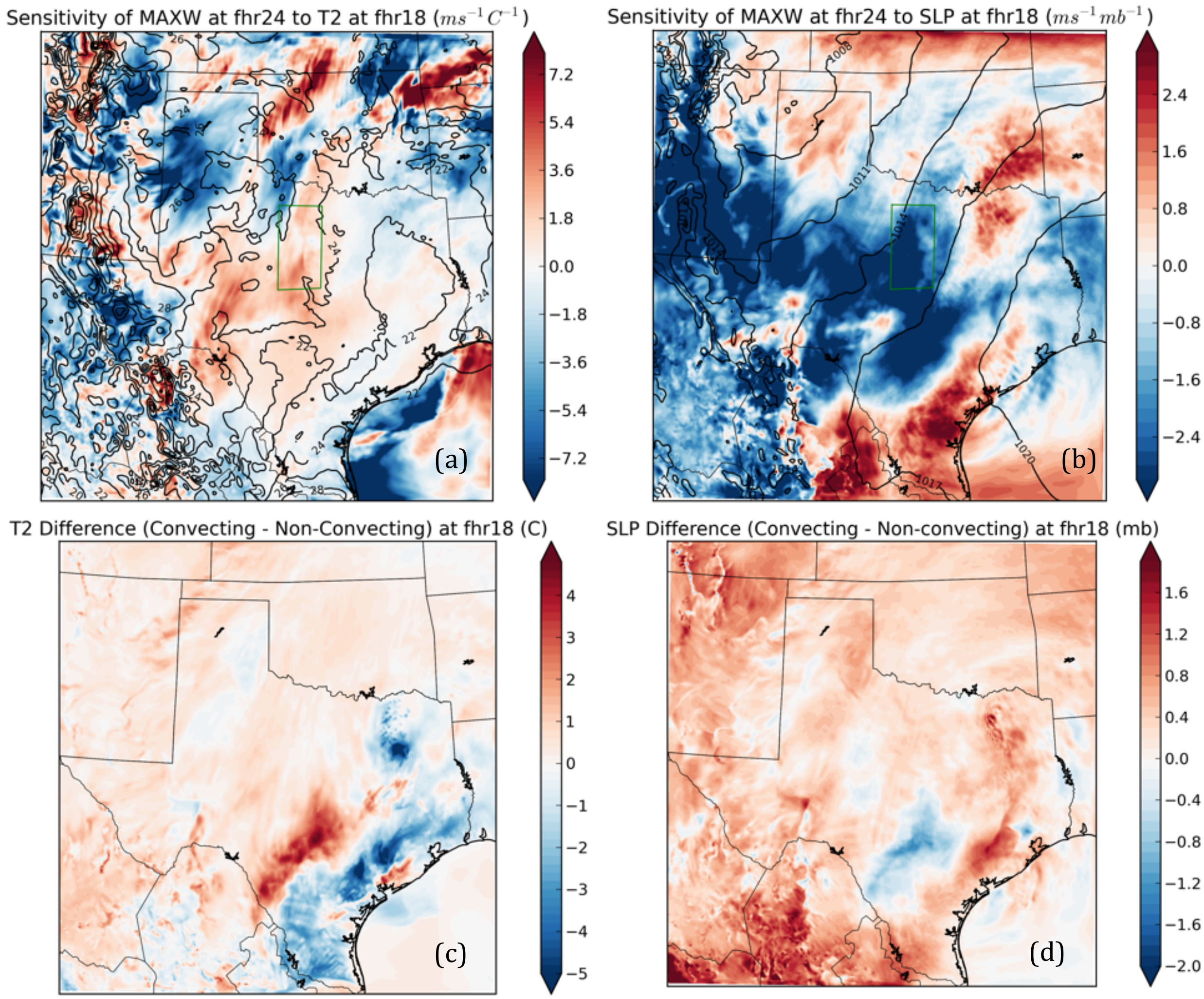

Figure 10 – Sensitivity of maximum vertical velocity at forecast hour 24 in the green rectangle to (a) 2-meter temperature (m s^{-1} $^{o}C^{-1}$, shaded) and (b) sea level pressure (m s^{-1} mb^{-1}, shaded) at forecast hour 18. Ensemble mean fields are contoured every 2 ^{o}C and 3 mb, respectively. (c) 2-meter temperature (^{o}C, shaded) and (d) sea level pressure (mb, shaded) difference between a chosen convecting and non-convecting member at forecast hour 18.

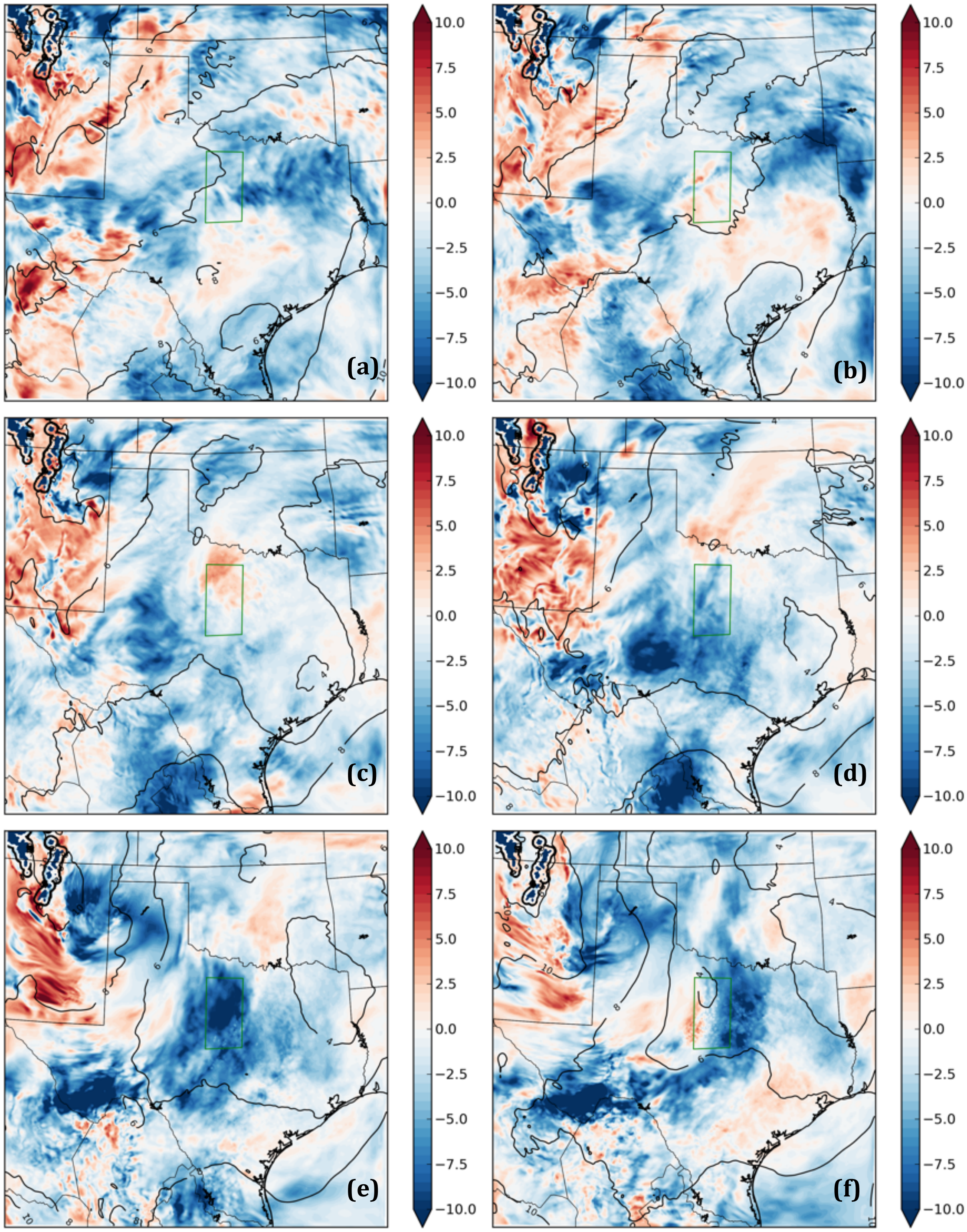

Figure 11 – Sensitivity of maximum vertical velocity at forecast hour 24 in the green rectangle area to 700 mb temperature (m s^{-1} $^{o}C^{-1}$, shaded) at forecast hours (a) 9, (b) 12, (c) 15, (d) 18, (e) 21, and (f) 24. Ensemble mean temperature contoured every 2 ^{o}C.

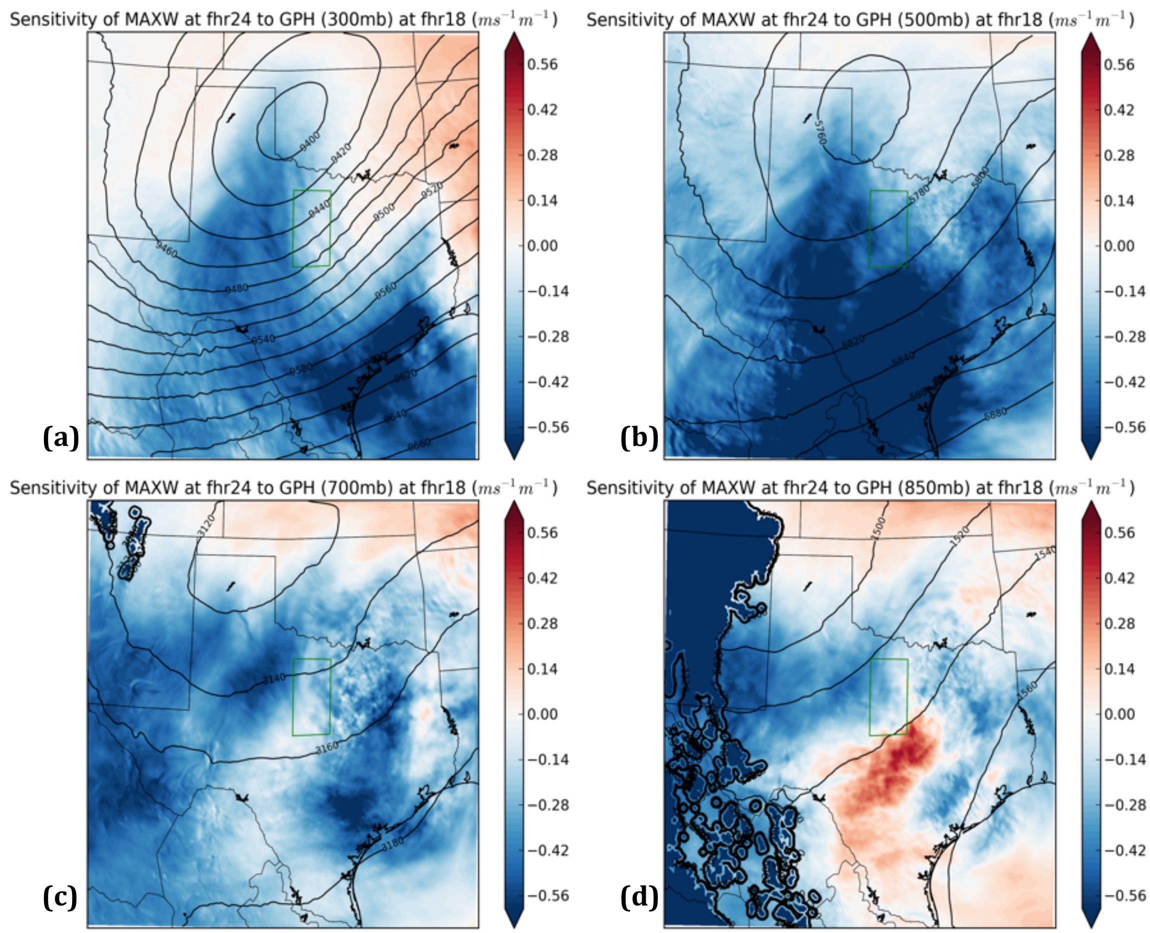

Figure 12 - Sensitivity of maximum vertical velocity at forecast hour 24 in the green rectangle area to (a) 300, (b) 500, (c) 700, and (d) 850 mb geopotential height ($m\ s^{-1}\ m^{-1}$) at forecast hour 18. Ensemble mean geopotential heights are contoured every 20 m.

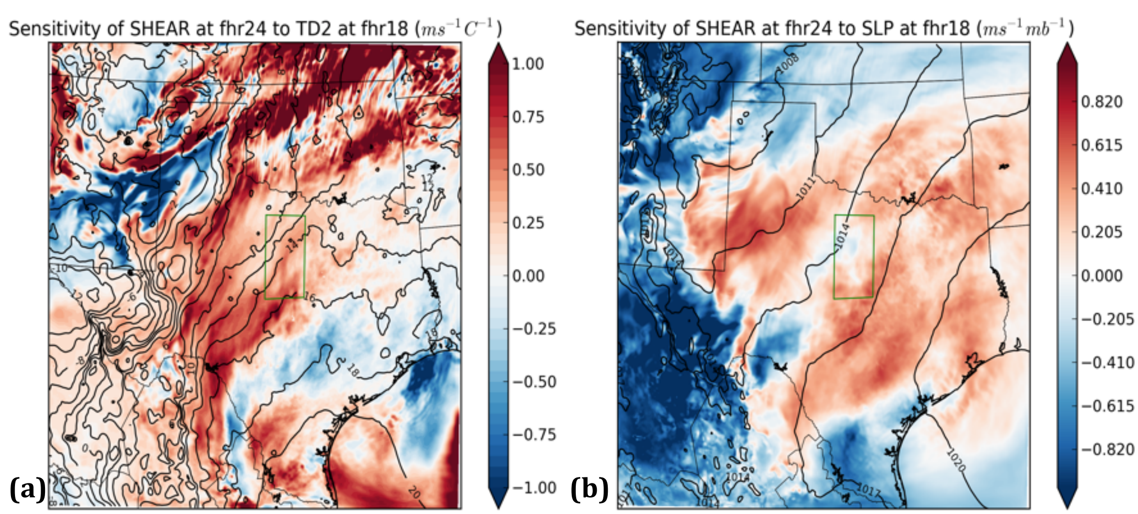

Figure 13 – Sensitivity of average bulk shear at forecast hour 24 in the green rectangle area to (a) 2-meter dewpoint (m s^{-1} $^{o}C^{-1}$, shaded) and (b) sea level pressure (m s^{-1} mb^{-1}) at forecast hour 18. Ensemble mean fields are contoured every 2 ^{o}C and 3 mb, respectively.

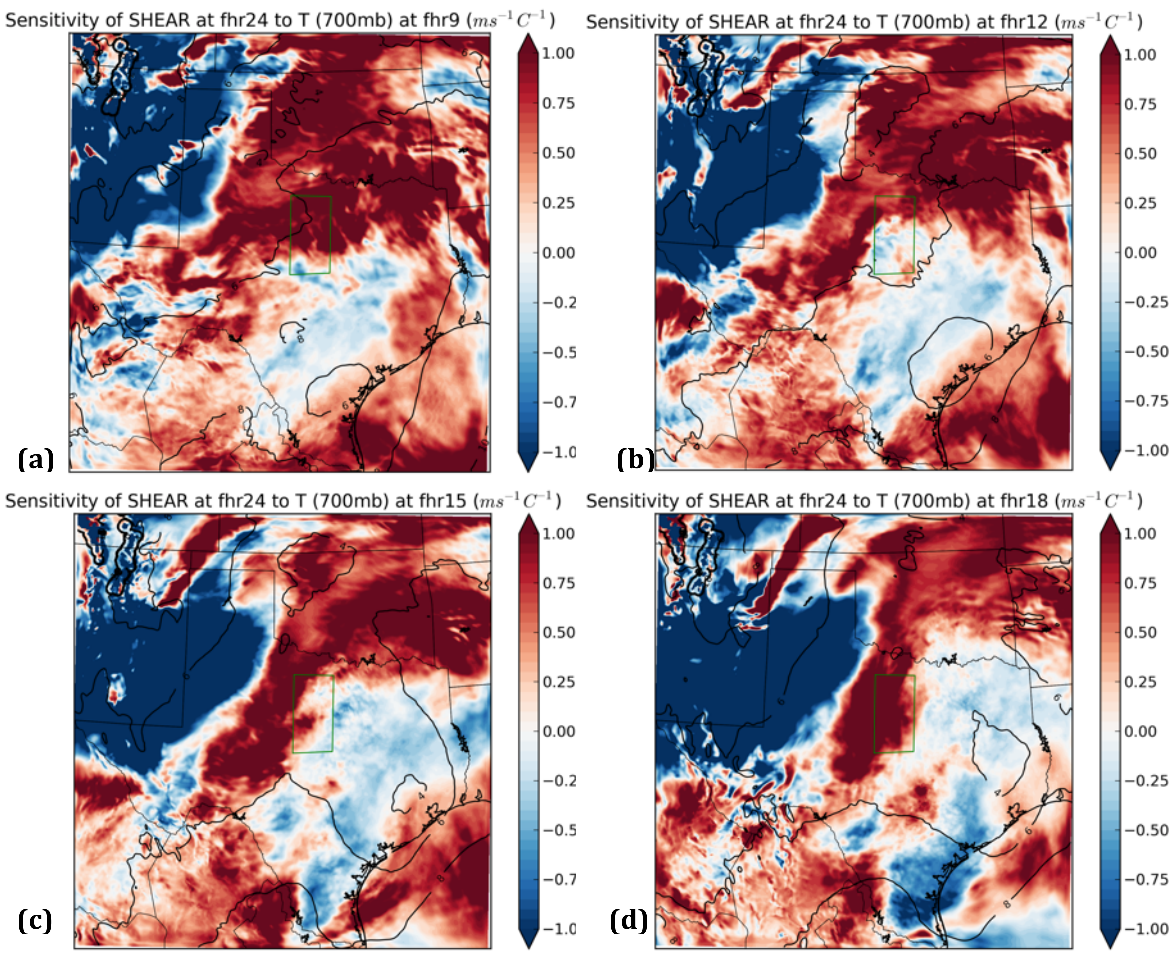

Figure 14 – Sensitivity of average bulk shear at forecast hour 24 in the green rectangle area to 700 mb temperature (m s^{-1} $^{o}C^{-1}$, shaded) at forecast hours (a) 9, (b) 12, (c) 15, and (d) 18. Ensemble mean temperature contoured every 2 ^{o}C.

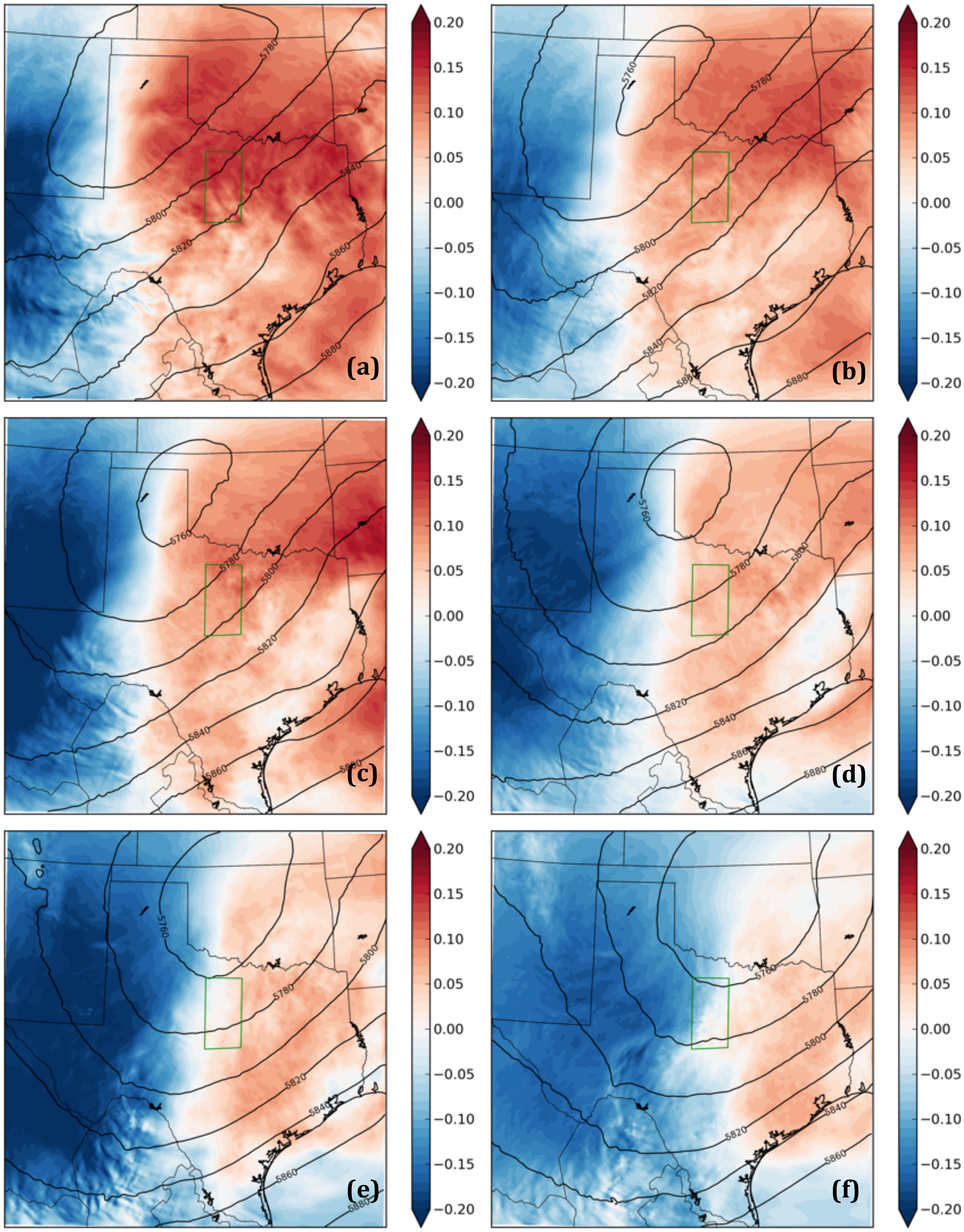

Figure 15 - Sensitivity of average bulk shear at forecast hour 24 in the green rectangle area to 500 mb geopotential height (m $s^{-1}m^{-1}$, shaded) at forecast hours (a) 9, (b) 12, (c) 15, (d) 18, (e) 21, and (f) 24. Ensemble mean heights contoured every 20 m.